Nature Communications

https://doi.org/10.1038/s41467-026-69033-8

Article in Press

In vivo dual RNA-Seq uncovers key effectors of epithelial barrier disruption by an extracellular pathogen

Received: 15 April 2025

Accepted: 22 January 2026

Cite this article as: Giraud-Gatineau, A., Haustant, G., Monot, M. *et al.* In vivo dual RNA-Seq uncovers key effectors of epithelial barrier disruption by an extracellular pathogen. *Nat Commun* (2026). https://doi.org/10.1038/s41467-026-69033-8

Alexandre Giraud-Gatineau, Georges Haustant, Marc Monot, Mathieu Picardeau & Nadia Benaroudj

In vivo Dual RNA-Seq uncovers key effectors of epithelial barrier disruption by an extracellular pathogen

Alexandre GIRAUD-GATINEAU[1]*, Georges HAUSTANT[2], Marc MONOT[2], Mathieu PICARDEAU[1], Nadia BENAROUDJ[1]*

[1] Biology of Spirochetes, Institut Pasteur, Université Paris Cité, CNRS UMR 6047, F-75015 Paris, France.

[2] Plate-forme Technologique Biomics, Institut Pasteur, Université Paris Cité, F-75015 Paris, France

*For correspondence: nadia.benaroudj@pasteur.fr, agiraudg@pasteur.fr

ABSTRACT

Disruption of host cell barriers is a fundamental strategy enabling pathogens to establish a paracellular infection. Here, using dual RNA-Seq, we determine the *in vivo* host-pathogen transcriptomic landscape upon infection by the extracellular pathogen *Leptospira interrogans* and uncover a mechanism of cell-cell junction disruption. We demonstrate that, upon infection, an increase in intracellular calcium triggers tight junction destabilization, by activating the calmodulin and myosin light chain kinase signalization. We identify two bacterial effectors of the Virulence-Modifying (VM) proteins family, structurally related to toxin-like proteins, that promote modulation of calcium homeostasis and disruption of cell-cell junctions, thereby allowing *Leptospira* translocation across epithelium barriers, tissue colonization and pathogenicity. Furthermore, we demonstrate that at least one of these VM proteins is secreted and associates with host cells. Altogether, these findings reveal a unique strategy by which an extracellular pathogen secretes toxin-like proteins to exploit host calcium signaling for breaching epithelial barriers.

INTRODUCTION

Successful microbial infection and host colonization depend on the ability of pathogens to evade, resist and/or manipulate host defenses. While much of our understanding of mechanisms underlying the dynamic interplay between a host and a pathogen (i. e. host-pathogen interactions) stems from studies on well-characterized intracellular and extracellular pathogens, our understanding remains incomplete for many extracellular species that lack canonical virulence factors. Moreover, these interactions have been generally investigated under *in vitro* condition that cannot fully replicate the complexity of a living host.

A critical feature to establish infection is the ability of extracellular pathogens to compromise the integrity of endothelial and epithelial barriers[1], which are vital for maintaining organ integrity. Tissue integrity depends on protein scaffolds stabilizing cell-cell junctions, including tight junctions (TJs) and adherens junctions (AJs). TJs are formed by claudin, occludin, JAM-1 and zonula occludens (ZO) proteins while AJs are constituted of the calcium-binding protein cadherin[2]. Both TJs and AJs interact with the actin cytoskeleton to maintain barrier integrity. Pathogens often disrupt these junctions, directly or indirectly, through cytoskeletal regulation to invade a host[3]. Although several bacterial toxins and effectors from well-studied extracellular pathogens have been shown to disrupt cell-cell junctions, the detailed molecular mechanisms underlying junction disruption remain poorly understood for a variety of bacteria.

Among extracellular pathogens, *Leptospira* spp., the causative agents of leptospirosis, have evolved strategies to breach these barriers and disseminate throughout the host. These bacteria enter through skin abrasion or mucosa, evade the innate immune response and rapidly disseminate hematogenously to organs, including kidneys and liver, resulting in multiple organ failure and hemorrhage. With an estimated one million severe cases and 60,000 deaths reported annually[4], leptospirosis is the most widespread zoonotic disease. Previous studies have demonstrated that *L. interrogans* infect their mammalian host through a paracellular route, disrupting both TJs and AJs[5,6]. Because *Leptospira* exclusively employs a paracellular route to colonize host tissues, it served as an ideal model to understand mechanisms of cell-cell junction disruption by extracellular pathogens.

Here, we developed a dedicated protocol for dual RNA-Seq profiling of *L. interrogans*-infected hamsters, a model of human acute leptospirosis, to elucidate how this extracellular pathogen spreads and compromises cell barrier integrity. Transcriptional host response was characterized by alterations in pathways associated with paracellular permeability, including cell-cell junctions and cytoskeletal organization. We demonstrated that the disruption of cell-cell

junctions by *L. interrogans* correlated with calcium homeostasis deregulation and activation of calmodulin and MLCK kinases. Obtaining the *in vivo L. interrogans* transcriptomic profile allowed for the identification of two leptospiral toxin-like proteins of the Virulence-Modifying (VM) family. We established their essentiality in *Leptospira* pathogenicity and their involvement in regulating the calcium-induced calmodulin/MLCK signaling pathway, leading to cell-cell junction disassembly and promoting paracellular transmigration through host tissues. These findings revealed a unique mechanism by which an extracellular pathogen alters host calcium signaling to disrupt cell barriers for facilitating its dissemination and colonization inside the host.

RESULTS

Dual RNA-Seq of *L. interrogans*-infected hamsters

To define the optimal condition for performing dual RNA-Seq in the model of human acute leptospirosis, Golden Syrian hamsters were infected with 10^8 *L. interrogans* by intraperitoneal route. This model was previously described to ensure reproducible susceptibility to lethal *Leptospira* infection and to reliably induce severe multi-organ pathology of human leptospirosis[7–9]. In these conditions, colonization of *L. interrogans* was detectable in liver and kidneys at 1-day post-infection (dpi), with signs of morbidity apparent at 4 dpi (**Fig. 1A-B**). To assess transcriptional changes at early and late stages of infection, we performed RNA sequencing of the host and *Leptospira* on liver and kidney tissues collected at 1 and 3 dpi (**Fig. 1C**). Initial sequencing, performed at standard read depths (~40 million reads/sample), revealed that more than 99.9% of total reads mapped to hamster genome, allowing for the identification of up to 984 differentially expressed genes (DEGs, *p.adj* < 0.05; $|Log_2FC| > 1$) (**Fig 1D**, **Supplementary Fig. 1A**). Among all conditions tested, the highest proportion of *Leptospira* reads was obtained by sequencing RNAs isolated from liver tissue at 3 dpi, detecting the expression of only 85 *Leptospira* genes (**Supplementary Fig. 1A**). To overcome this limitation and achieve higher *Leptospira* transcriptome coverage, RNAs isolated from liver at 3 dpi were deep-sequenced (~400 million reads/sample). This approach significantly increased the proportion of *Leptospira* genes detected from 4.57% of all expressed genes encoded in the bacterial genome to 79.34%, with a robust and well-distributed read count across *Leptospira* genome (**Fig. 1E, Supplementary Fig. 1B-E**). Thus, this experimental design provides a comprehensive and robust dual RNA sequencing profile encompassing both the host and pathogen transcriptomic responses.

Transcriptomic host response upon *Leptospira* infection

Principal component analysis (PCA) of the RNA-Seq data set revealed distinct clustering of infected compared to uninfected samples at 3 dpi, while no separation was observed at 1 dpi, in liver as well as in kidney tissues (**Fig. 1D**). Despite the detection of a significant *L. interrogans* load at 1 dpi (**Fig. 1B**), the host transcriptional response was minimal, with only 4 and 8 DEGs (*p.adj* < 0.05; $|Log_2FC|$ >1) in the liver and kidneys, respectively (**Fig. 1D, Supplementary Fig. 2A**, **Supplementary Data 1**). By 3 dpi, the transcriptional response was increased significantly, with 984 and 72 DEGs (*p.adj* < 0.05; $|Log_2FC|$ >1) in the liver and kidneys, respectively (**Fig. 1D**, **Supplementary Fig. 2A**, **Supplementary Data 1**). These findings indicate that *L. interrogans* do not elicit an early host transcriptional response, even at a high infectious dose (10^8), given a LD50 of 10-100 leptospires[10].

At 3 dpi, both liver and kidney exhibited transcriptional changes associated with inflammation, cell-cell junctions, and cytoskeletal organization (**Fig. 2A**, **Supplementary Fig. 2B-D and Supplementary Data 2**). Pathway enrichment analysis revealed upregulation of cytokine-cytokine receptor interaction (e.g., *gdf15*, *ccl2*, *cxcl10*, *il1b*) and chemokine signaling (*fgr*, *hck*, *stat3*), highlighting a common inflammatory response in both organs (**Fig. 2B**). Genes involved in the actin cytoskeleton, focal adhesions, tight junctions, and cell adhesion were also upregulated, including genes encoding integrins (*itgal* in both liver and kidney; *itgb6*, *itgav*, *itga5*, *itga3* in liver; and *itga4*, *itga8* in kidney), as well as actin-related proteins (*mlck*, *actg1* in liver; *mapk3*, *pip5k1n* in kidneys; **Fig. 2C Supplementary Fig. 2B-D and Supplementary Data 2**). The differential expression of genes involved in inflammation (*cxcl10*, *ccl2*, *fgr*, *nfκb1*), calcium signaling (*cd38*, *mcoln2*, *mylk*, *calm1*), and actin/cell-cell junction (*actb*, *itgal*, *arpc1b*, *jun*, *tjp2*, *cdh1*) in liver and/or kidney were confirmed by RT-qPCR (**Supplementary Fig. 2E-F**).

In addition to the transcriptional responses shared by the liver and kidneys, organ-specific differences emerged. In the liver, transcriptional changes were more pronounced, with strong upregulation of inflammatory pathways, protein processing in the endoplasmic reticulum and cell-cell junction pathways (**Fig. 2A**, **Supplementary Fig. 2 and Supplementary Data 2**). In addition, we observed an upregulation of the calcium signaling pathway and genes encoding factors related to cell-cell junction integrity such as cadherin (*cdh1*) and tight junction protein (*tjp2*, encoding ZO-2). In contrast, the kidneys showed a more restricted transcriptional response, with fewer differentially expressed genes (**Fig. 1D**). A key distinction was the downregulation of specific metabolism-related pathways in the two organs. The liver response showed a specific downregulation of amino acid and fatty acid metabolism, whereas the kidney response was associated with a downregulation of oxidative phosphorylation (**Fig. 2A**, **Supplementary Fig. 2**

and Supplementary Data 2). Taken together, these findings indicate that, upon leptospiral infection, while both organs activate the inflammatory response and cell-cell junction pathways, the liver undergoes a more extensive transcriptional shift.

***Leptospira* transcriptional profile *in vivo*.**

Analysis of the transcriptomic response of *L. interrogans* in liver of infected hamsters showed that the expression of 1685 *Leptospira* genes (59% of total ORFs) was affected *in vivo* compared to *in vitro* condition, with 352 and 1333 up- and downregulated genes (*p.adj* <0.05; $|Log_2FC| > 1$), respectively (**Fig. 3A**, **Supplementary Data 3**). Pathway enrichment analysis indicated that upregulated genes were predominantly linked to bacterial secretion system, O-antigen biosynthesis and key metabolic pathways such as carbon, amino acid, and porphyrin metabolisms (**Fig. 3B**, **Supplementary Fig. 3 and Supplementary Data 4**). Notably, several genes encoding molecular chaperones involved in the proteotoxic stress response, such as *groES, groEL*, *hsp15*, *hsp20*, *dnaK*, *dnaJ*, and *grpE* were among the most highly upregulated (**Fig. 3C**). Additionally, the expression of several virulence-associated genes was significantly increased, including two genes encoding members of the Virulence-Modifying (VM) family, *sph* genes (encoding sphingomyelinase C), *ligA* and *ligB* (coding for immunoglobulin-like proteins A and B), *colA* (encoding collagenase A) and *LIMLP_09380* (encoding a hypothetical membrane protein)[11].

By contrast, genes involved in flagellar assembly, bacterial chemotaxis and two-component systems were downregulated (**Fig. 3B**, **Supplementary Fig. 3**). This included the decreased expression of a cluster (*LIMLP_07420-07460*) containing several genes associated with chemotaxis, such as *mcpa* and *cheABDRWY* and of several histidine kinase-encoding genes (*LIMLP_11010*, *LIMLP_10185*, *LIMLP_10190*, *LIMLP_16820*) (**Fig. 3C**). In addition, we observed the downregulation of genes associated with lipid, carbohydrate and coenzyme transport and metabolism (**Supplementary Data 4**).

Altogether, these findings revealed a major transcriptional reprogramming of *L. interrogans in vivo*, highlighting stress adaptation, metabolic shift and virulence induction as key features of adaptation to the host environment.

***L. interrogans* induces actin reorganization and disrupts epithelial cell junctions in the host.**

The host transcriptional response suggested cell-cell junction regulation during leptospiral infection. We evaluated whether changes in expression of genes involved in this process

correlated with F-actin rearrangement and cell junction disruption in human epithelial cells infected by *L. interrogans*. Live-cell and immunofluorescence microscopy showed that human epithelial cells infected with *L. interrogans* exhibited dispersion and a less expanded morphology with actin staining at 24 hr pi, resulting in reduced cell-cell contacts (**Fig. 4A-C**). Such phenomenon was not observed in cells infected with the saprophytic species *L. biflexa* (**Supplementary Fig. 4**). Importantly, no epithelial cell death was observed for at least 48 hr pi (**Fig. 4D, Supplementary Fig. 5A**), indicating that actin rearrangement was not related to cell death. Immunoblot analysis showed increased cellular contents of actin nucleation and polymerization factors (Profilin-1, WAVE-2, and phosphorylated-Rac1), as well as of the actin reorganization factor phosphorylated Cofilin (**Supplementary Fig. 5B**). Of note, genes encoding these factors were upregulated upon *Leptospira* infection in liver (**Supplementary Table 1**).

In addition, infected cells exhibited at 24 hr pi a decrease of cadherin protein in plasma membrane (1.6-fold reduction) (**Fig. 5A**) and a reduction in tight junction proteins ZO-1, ZO-2, and JAM-1 compared to uninfected controls (1.5-, 1.4- and 1.6-fold reductions for ZO-1, ZO-2 and JAM-1, respectively, as measured by immunofluorescence, **Fig. 5B-C**). Decrease in ZO-1 and ZO-2 was also observed by immunoblot (**Fig. 5D**). Experiments using the human hepatic cell line HepG2 confirmed these observations, showing no cell death upon *L. interrogans* infection together with decreased cadherin at the plasma membrane and reduced ZO-1 levels (**Supplementary Fig. 6**). Interestingly, infection by *L. interrogans* did not lead to a decrease of the gap junction protein Connexin-43 cellular content but to a change in its localization. Indeed, while Connexin-43 was primarily localized at the plasma membrane in uninfected cells, it accumulated in the endoplasmic reticulum (ER) in infected cells (**Fig. 5E-G**). Finally, disruption of cell junctions upon infection by *L. interrogans* correlated with a greater ability to cross epithelial monolayers, compared with the saprophytic *L. biflexa* which lacks the capacity to disrupt cell-cell junction integrity (**Fig. 5H** and **Supplementary Fig. 4**). Altogether, these results demonstrate that infection by *L. interrogans* leads to a profound reorganization of the cytoskeleton and compromises epithelial barrier integrity probably by triggering downregulation or mislocalization of tight, adherens and gap junction proteins.

ER stress response and its implications in *Leptospira*-infected cells

The host transcriptional response and RT-qPCR analysis under *in vitro* condition revealed an upregulation of genes associated with the ER stress pathway during infection by *L. interrogans* (**Fig. 2A** and **Supplementary Fig. 7A-B**). Given the correlation between ER stress and the disruption of cell-cell junctions[12–14], we evaluated the modulation of ER activity upon infection by

L. interrogans. Using a fluorescent ER marker specific to the ATP-sensitive K^+ channels of this organelle, we observed reduced signal intensity at 6, 24 and 48 hr pi in infected cells (**Supplementary Fig. 7C-D**) with increased phosphorylation of PERK and IRE-1 (**Supplementary Fig. 7E**), suggesting altered ER function. To determine whether this ER stress response contributed to cell junction disruption, infected cells were treated with different ER stress inhibitors. However, none of the inhibitors restored cell-cell junction integrity in *L. interrogans*-infected cells (**Supplementary Fig. 7F-G**). Therefore, while *L. interrogans* induces an ER stress response probably mediated by PERK and IRE-1 pathways, this response does not substantially contribute to cell-cell junction disruption.

Calcium signaling participates in cell-cell junction disruption in *L. interrogans*-infected cells

Given the upregulation of calcium-related genes upon *L. interrogans* infection (**Fig. 2A and 2C**) and the established role of Ca^{2+} signaling in cytoskeletal dynamics[15], we investigated whether this cation contributed to cell-cell junction disruption. Intracellular Ca^{2+} levels increased by 1.65- and 1.39-fold in infected epithelial cells at 24 and 48 hr pi, respectively, compared to uninfected controls (**Fig. 6**). To determine whether this Ca^{2+} accumulation was functionally linked to junction disruption, we treated infected cells with BAPTA-AM, a cell-permeable Ca^{2+} chelator. This treatment effectively limited the infection-induced Ca^{2+} increase, reduced cell junction dispersion and increased ZO-1 and cadherin localization at cell-cell junctions compared to untreated infected cells (**Fig. 7A-C, Supplementary Fig. 8, Supplementary Fig. 9A**). These results suggest that intracellular Ca^{2+} plays an important role in *Leptospira*-induced junction disruption.

TJ and AJ integrity depends on the interaction between the TJ or AJ protein complexes and the perijunctional actomyosin ring[16], a process controlled by calmodulin-dependent myosin light chain kinase (MLCK) activity. MLCK activation leads to myosin phosphorylation, resulting in increased cell junctions permeability in epithelial cells[17,18]. *L. interrogans*-infected epithelial cells exhibited elevated level of phosphorylated myosin compared to uninfected controls (**Fig. 7D**). Inhibition of calmodulin or MLCK using KN-93 or ML-7 inhibitors, respectively, partially restored ZO-1 and cadherin localization at cell-cell junctions and reduced cell dispersion in infected cells (**Fig. 7E-G, Supplementary Fig. 9B)**. Notably, this inhibition also impaired *L. interrogans* transmigration across the epithelial monolayer (**Fig. 7H**). These findings indicate that *L. interrogans* exploits host Ca^{2+} signaling to activate the calmodulin-MLCK pathway, leading to junctional disassembly and enhanced paracellular transmigration.

Two *Leptospira* Virulence-Modifying (VM) proteins are required for virulence and disruption of cell-cell junction through calcium signaling pathway

The most highly upregulated leptospiral genes *in vivo* encode two Virulence-Modifying (VM) proteins (*LIMLP_11655*, $Log_2FC=7.9$; *LIMLP_11660*, $Log_2FC=8.9$; **Fig. 3A**, **Supplementary Data 3**). These VM proteins belong to the DUF1561 family, whose function remains unknown. They possess toxin-like features, including a ricin B-like (or Cards B-like) domain potentially mediating interaction with host receptors, and a C-terminal domain of unknown function[19] (**Supplementary Fig. 10A)**. In *L. interrogans*, *LIMLP_11655* and *LIMLP_11660* genes are adjacent (**Supplementary Fig. 10B).**

Orthologs of VMs are present in other pathogenic bacteria such as *Bartonella*, *Helicobacter* and *Campylobacter* (**Supplementary Fig. 10C-E**). *L. interrogans* harbors a total of thirteen VM proteins, all exclusive to pathogenic *Leptospira* species[11]. Comparative sequence identity analyses indicated that LIMLP_11655 and LIMLP_11660 exhibit greater sequence similarity to each other than to other VM proteins (**Supplementary Fig. 10F)**. Notably, LIMLP_11655 and LIMLP_11660 were the only two VM genes significantly upregulated *in vivo* (**Supplementary Fig. 10F**).

We had already demonstrated that silencing *LIMLP_11655* (hereafter referred to as *dcas9-LIMLP_11655* mutant) led to an attenuated *L. interrogans* virulence in hamsters[11]. Likewise, *LIMLP_11660* inactivation led to complete loss of virulence, which was restored upon complementation (**Fig. 8**). Furthermore, when both VM genes were inactivated or silenced, (hereafter referred to as *LIMLP_11660+dcas9-LIMLP_11655 mutant*), *L. interrogans* virulence was lost. Importantly, all these strains exhibited growth rates comparable to that of the WT when cultivated in EMJH medium (**Supplementary Fig. 11**), ensuring that the observed decreased virulence could not be attributed to growth defects. Additionally, all three mutants (*LIMLP_11660*, *dcas9-LIMLP_11655* and *LIMLP_11660+dcas9-LIMLP_11655*) exhibited a reduced ability to transmigrate across epithelial cells at 3 hr pi (**Fig. 9A**).

To investigate whether LIMLP_11660 and LIMLP_11655 contribute to epithelial cell barrier disruption as secreted factors, we tested whether supernatants from WT and mutant strains (*LIMLP_11660*, dcas9-*LIMLP_11655*, and *LIMLP_11660*+dcas9-*LIMLP_11655*) could promote the transmigration of saprophytic *L. biflexa*, normally unable of crossing the epithelial barrier (as seen in **Fig. 5H**). Incubation of epithelial cells with *L. interrogans* WT supernatant enhanced *L. biflexa* translocation, indicating that *L. interrogans* secretes factors capable of disrupting epithelial junctions (**Fig. 9B**). Conversely, supernatants from VM mutants (*LIMLP_11660*, *dcas9-LIMLP_11655* and *LIMLP_11660+dcas9-LIMLP_11655*) exhibited a lower ability to promote *L.*

biflexa transmigration and to reduce cadherin and ZO-1 levels at epithelial junctions (**Fig. 9B-C, Supplementary Fig. 12A**). Complementation of *LIMLP_11660* mutant restored both the ability to promote *L. biflexa* transmigration as well as reduced cadherin and ZO-1 amounts at the cell-cell junction to a comparable manner as the WT (**Fig. 9B-C**, **Supplementary Fig. 12A**). However, infection with VM mutants still led to the disruption of cadherin and ZO-1 in epithelial cells (**Supplementary Fig. 12B-C**), except for the *LIMLP_11660*+dcas9-*LIMLP_11655* mutant where we observed a slight increase of cadherin and ZO-1 localization in cell junction. Similar alterations were also observed in hepatocyte cells using incubation with supernatants or bacterial infection (**Supplementary Fig. 13**).

To confirm VM secretion, we complemented the *LIMLP_11660* mutant with a Flag-tagged allele (*LIMLP_11660*$_{comp\text{-}C1}$) and we successfully detected the Flag-tagged LIMLP_11660 protein in the *L. interrogans* supernatant (**Fig. 9D**). Furthermore, when epithelial cells were exposed to the supernatant from *LIMLP_11660*$_{comp\text{-}C1}$ strain for 1 and 6 hr, the Flag-tagged protein was detected in a total lysate of the epithelial cells, and this correlated with a reduced ZO-1 amount at the cell-cell junction comparable to that observed upon incubation with the WT strain supernatant (**Fig. 9E, Supplementary Fig. 14**). These findings demonstrate that LIMLP_11660-encoded VM is secreted by *L. interrogans*, interacts with and modulates the host cell environment. These results suggest that these two VM proteins exert their role in *Leptospira* pathogenicity by being secreted, binding to the host cell plasma membrane, possibly by being internalized within host cells, disrupting TJ and AJ, and promoting *Leptospira* transmigrating through epithelial cells layers.

We next examined whether LIMLP_11660 and LIMLP_11655 promoted TJ and AJ disruption by altering Ca^{2+}-calmodulin-MLCK signaling. Incubation with supernatants of *LIMLP_11660* or *dcas9-LIMLP_11655* mutant cultures significantly impaired the rise of intracellular Ca^{2+} concentration by 4 and 8.5 times, respectively, compared to WT. *LIMLP_11660* complementation restored the increase in intracellular Ca^{2+} concentration observed upon incubation with the supernatant of WT (**Fig. 9F**, **Supplementary Fig. 15A)**. Of note, these effects were less pronounced when infecting epithelial cells with corresponding whole bacterial strains (**Supplementary Fig. 15B**). Moreover, incubating cells with supernatants from VM mutant cultures correlated with reduced phosphorylation of myosin, a mediator of TJ and AJ integrity (**Supplementary Fig. 16)**. Collectively, these findings demonstrate that LIMLP_11660 and LIMLP_11655 act upstream of the Ca^{2+}-calmodulin-MLCK pathway, facilitating TJ and AJ disruption through calcium signaling activation.

DISCUSSION

Dual RNA-seq has emerged as a powerful tool to unravel the complex interactions between a host and its pathogen(s), enabling comprehensive understanding of essential biological processes in both organisms during infection. However, its *in vivo* application presents significant technical challenges due to the low bacterial/host RNA ratio, particularly with strict extracellular pathogens where specific selection of infected cells cannot be used. Through advances in high-throughput sequencing technologies, we overcame these obstacles. A deep sequencing approach allowed obtaining robust dual RNA-seq datasets from infected hamsters. This strategy enhanced the coverage of *L. interrogans* transcripts without introducing external factors that might interfere with the host-pathogen dynamics. This refined approach led to valuable insights into the interaction between a host and an extracellular pathogen, providing a framework for studying the molecular mechanisms that drive acute bacterial infection *in vivo*.

The present study demonstrates that, despite *Leptospira* colonizing organs within the first hour of infection[20], a low transcriptional host response is observed during the first 24 hr of infection. This lack of early response is particularly striking when compared to other bacterial infections, where early transcriptional responses encompasses about 1,971 DEGs in average across diverse pathogens, regardless of their extracellular or intracellular nature[21–26] (**Supplementary Table 2**). The low transcriptional host response at the early stage of infection observed here is consistent with the stealth strategy used by pathogenic *Leptospira* to evade host recognition, a key process that favors bacterial dissemination. Indeed, unlike most pathogens, which promptly elicit a strong inflammatory response, *Leptospira* can evade complement-mediated killing[27], recognition by Toll-like receptor[28], and internalization by macrophages[11,29]. However, this initial immune evasion is eventually counteracted as the infection progresses. At 3 dpi, the host transcriptomic profile demonstrated a significant upregulation of inflammatory mediators, notably cytokine-cytokine receptor interactions and NF-κB signaling pathways. Among these, genes such as *ccl3*, *cxcl10*, *ccl2*, *tnf*, and *il1β* were highly induced, aligning with previous reports that have implicated these cytokines as potential biomarkers for severe leptospirosis in patients[30–32]. Importantly, our analysis also revealed the upregulation of chemokines and cytokines not previously associated with *L. interrogans* infection, including GDG15 (Growth differentiation factor 15) and CCL4 (also called MIP-1β), which are known to be induced during systemic bacterial infections and sepsis[33,34]. Identifying such biomarkers not only enhances our

understanding of the molecular mechanisms of bacterial infection but may also improve diagnosis, which remains challenging, and patient outcomes of this treatable infection.

The liver and the kidney exhibited distinct transcriptomic responses to *L. interrogans* infection, highlighting the importance of organ-specific immune and metabolic adaptations during bacterial colonization. The liver showed a strong upregulation of inflammatory pathways, calcium signaling and cell junction-related genes, probably due to a higher bacterial load (**Fig. 1B**) and extensive vascularization. If so, organ perfusion prior to RNA isolation would allow eliminating such bias. Nevertheless, the attenuated response of kidney observed here could reflect the limited immune cell infiltration of renal proximal tubules, a primary site of *Leptospira* persistence. This strategy would be similar to pathogens, such as *Mycobacterium tuberculosis*[35] or *Brucella*[36], that exploit immune-privileged niches to establish long-term colonization. In addition, including blood samples in the dual RNA-seq analysis, alongside liver and kidney tissues, would provide a broader overview of the host response to *Leptospira* infection. Blood transcriptomic profiling could offer valuable insights into the systemic immune response and help to determine whether the limited inflammatory response observed at early infection stages is also reflected in circulating immune cells. Moreover, as lungs are also a site of *Leptospira* infection, determining the transcriptomic profile of *Leptospira*-infected lung tissues could shed some light on severe pulmonary haemorrhagic syndrome associated with leptospirosis.

Breaking the epithelial barrier is a critical step in bacterial pathogenesis but the underlying host-pathogen interactions remain poorly understood, as studies often focus on bacterial factors or the downstream consequences of barrier disruption rather than the molecular mechanisms driving these processes[37]. Here, we found that several genes related to actin and myosin cytoskeleton, tight and adherens junctions and cell adhesion were upregulated upon infection by *Leptospira*, which is consistent with cell-cell disruption favoring dissemination by a paracellular route[5,38]. Such gene regulations were not observed upon infection by *Salmonella enterica* and *Listeria monocytogenes*, although these pathogens use the paracellular route[22,39]. However, the absence of regulation in cell-cell junction pathway in these bacteria is likely due to their ability to exploit additional mechanisms for host invasion and dissemination. This probably reflects the importance of paracellular route in leptospiral infection.

We demonstrate here that, upon infection by *Leptospira*, modulation of expression of genes related to the transmigration pathway correlated with alterations in intracellular calcium concentration and activation of the MLCK-calmodulin pathway, two processes participating in disruption of cellular junctions. These findings align with a recent study suggesting that the ROCK

protein plays a role in E-cadherin disruption in endothelial cells, where ROCK, like MLCK, could induce myosin phosphorylation[38,40].

Importantly, we could identify in the present study two proteins from the VM family, LIMLP_11660 and LIMLP_11655, as key effectors promoting bacterial dissemination through activation of the Ca^{2+}-MLCK-Myosin pathway-induced cell-cell junction disruption. VM proteins exhibit structural features characteristic of AB toxin, a diverse class of bacterial virulence factors. The VMs family comprises 13 members in *Leptospira*, but their specific roles in pathogenicity remain unknown. It was previously showed that all VM genes were upregulated in the blood and liver of infected hamster at 4 dpi, but different expression levels were observed in the kidneys[41]. The two VMs studied here were the most highly expressed of the VMs in the condition used here. This suggests not only a temporal and tissue-specific expression pattern but also distinct function in infection. Even though some VMs may exhibit redundant activity, such as the two VMs identified here, others very likely contribute to different aspects of *Leptospira* pathogenesis, such as immune evasion, adhesion to host tissues, modulation of host signaling pathways or/and persistence in specific organs. Further functional characterization is required to elucidate the precise contributions of each VM in *Leptospira* virulence and dissemination. Transcriptomic variations may occur between *Leptospira* serovars or species with different host specificity and immune recognition. In this study, we used serovar Manilae, a well-established strain from the species *L. interrogans* that induces acute leptospirosis in hamsters. Other *L. interrogans* serovars from different serogroups are expected to show broadly similar dissemination patterns and transcriptional profiles, provided that the host remains susceptible and the strains encode homologs of the VM proteins identified here. Nevertheless, different serovars may differently modulate the early immune response, and more pronounced divergence would be observed with *Leptospira* species such as *L. borgpetersenii* or *L. kirschneri*.

Unlike most pathogenic diderm bacteria which encode type III and IV secretion systems to directly translocate effector proteins into the cytoplasm or plasma membrane of host cells[42], *Leptospira* encode only type I and II secretion systems. These systems are responsible for exporting proteins into the extracellular environment, suggesting a distinct strategy for host-pathogen interactions. Interestingly, leptospiral type I and II secretion systems were upregulated upon infection (as demonstrated in this study), suggesting a general role during infection and perhaps particularly in the secretion of virulence factors such as VMs.

By linking host calcium signaling and leptospiral VM-induced TJ disruption, we provide here a mechanism for bacterial pathogenesis. We propose that, once within the host, *Leptospira* induce the expression and secretion of these two VMs. These proteins interact with epithelial cells likely

by binding of their Ricin B domain to lectin receptors. The VMs would be then internalized inside host cells, and they would modulate calcium homeostasis, either directly or indirectly. This would result in the activation of the calmodulin-MLCK signaling pathway, ultimately leading to tight and adherens junction disassembly (**Fig. 10**). The loss of barrier integrity facilitates the translocation of *Leptospira* through epithelial and endothelial layers, promoting systemic dissemination to target organs.

Interestingly, VM proteins are not exclusive to pathogenic *Leptospira* but are also found in other pathogenic bacteria, including *H. pylori*, *C. jejuni* and *Bartonella*, which are known to target host cell-cell junctions for bacterial dissemination. VMs have never been studied nor characterized in these bacteria but they may function similarly to those in *L. interrogans*, by disrupting epithelial barriers through a host calcium homeostasis-controlled mechanism. In fact, this mechanism of cell-cell junction disruption may not be exclusive to *Leptospira* and could also be exploited by other pathogens, whether of bacterial, fungal or viral origin, to facilitate their dissemination across host barriers.

METHODS

Ethics Statement

Protocols for animal experiments are conformed to the guidelines of the Animal Care and Use Committees of the Institut Pasteur (Comité d'éthique d'expérimentation animale CETEA # 220016), agreed by the French Ministry of Agriculture. All animal procedures carried out in our study were performed in accordance with the European Union legislation for the protection of animals used for scientific purposes (Directive 2010/63/EU).

Bacterial strains and culture conditions

Strains and plasmids used in this study are listed in **Supplementary Tables 3 and 4**. WT *L. interrogans* serovar Manilae strain L495 and mutants, and WT *L. biflexa* serovar Patoc strain Patoc 1 (Paris strain), were cultivated aerobically in Ellighausen-McCullough-Johnson-Harris liquid medium (EMJH) at 30°C with shaking at 100 rpm. π1 and β2163 *E. coli* strains were cultivated in Luria-Bertani medium with shaking at 37°C in the presence of 0.3 mM thymidine or diaminopimelic acid (Sigma-Aldrich), respectively. Spectinomycin was added to the media at 50 µg/ml when needed.

In vivo animal infection

Four-week-old male Golden Syrian hamsters (RjHan:AURA, Janvier Labs) (n=4) were infected via intraperitoneal injection with 10^8 *L. interrogans* WT and mutant strains, with the number of bacteria enumerated using a Petroff-Hausser counting chamber. The animals were monitored daily and euthanized by carbon dioxide inhalation when they reached the predefined endpoint criteria (sign of distress). To assess leptospiral load, samples of kidney and liver tissue were harvested, and DNA was extracted using the Tissue DNA Purification kit (Maxwell, Promega). The bacterial burden and host DNA concentration were determined by quantitative polymerase chain reaction (qPCR) using the Sso Fast EvaGreen Supermix assay (Bio-Rad) with primers targeting the *flaB2* (LIMLP_09410) and *gapdh* genes, respectively (**Supplementary Table 5)**. The leptospiral load was expressed as genomic equivalents (GEq) per microgram of host DNA.

RNA extraction, library preparation and sequencing

Liver and kidneys tissues of hamsters (infected or not by *L. interrogans* as described above) were resuspended in the QIAzol lysis reagent (Qiagen) with 5 mm stainless-steel beads (Qiagen) and homogenized with the Qiagen TissueLyser (two cycles of one-minute at 25 Hz, with a one-minute break between cycles in ice). Total RNAs were extracted from homogenized samples using the RNeasy Mini Kit (Qiagen), with a DNAse digestion (Qiagen) incorporated in the protocol. RNAs were also isolated from exponentially growing *L. interrogans* cultivated in EMJH medium (10^{10} leptospires). Bacterial pellets were resuspended in the QIAzol lysis reagent and total RNAs were extracted using a similar procedure (RNeasy Mini Kit with a DNAse treatment). The quality of all RNA samples was evaluated using an Agilent 2100 bioanalyzer (Agilent Technologies) to ascertain a RNA integrity number (RIN) higher than 8.5.

Sequencing Libraries were constructed using an Illumina Stranded Total RNA Prep Ligation using the RibZero Plus kit (Illumina, USA) with custom primer design on rRNA following the supplier's recommendations. The efficiency of rRNA depletion for both *Leptospira* and hamster samples was evaluated by shallow sequencing, revealing residual rRNA levels of approximately 5% in *Leptospira* and 1–5% in hamster samples, confirming efficient depletion in both species. RNA sequencing was performed with the Illumina NextSeq 2000 and NovaSeq X+ platform for a target of 10M reads/sample for bacteria, 30M reads/sample for hamster and 400M reads/sample for deep sequencing (performed on RNA samples isolated from 3 hamsters infected by *L. interrogans*). The RNA-seq analysis was performed with Sequana 0.15.3[43] using the RNA-seq pipeline 0.16 (https://github.com/sequana/sequana_rnaseq) built on top of Snakemake 7.32.4[44]. Briefly, reads were trimmed from adapters using Fastp 0.22.0[45] then mapped to the *L. interrogans*

serovar Manilae genome (NZ_CP011931.1) and Golden Syrian hamsters genome (KB708127.1) using Bowtie2[46] and STAR[47]. FeatureCounts 2.0.1[48] was used to produce the count matrix, assigning reads to features using the corresponding annotation from Ensembl with strand-specificity information. To verify the absence of cross-mapping between host and pathogen reads, uninfected hamster RNA-seq libraries were aligned to the *L. interrogans* genome, which only yielded a few hits restricted to rRNA loci and no assignments to protein-coding genes, confirming the negligible cross-mapping. Quality control statistics were summarized using MultiQC 1.11[49]. Statistical analysis on the count matrix was performed to identify differentially regulated genes. Clustering of transcriptomic profiles were assessed using a Principal Component Analysis (PCA). Differential expression testing was conducted using DESeq2 library 1.34.0[50] scripts indicating the significance (Benjamini-Hochberg adjusted p-values, false discovery rate FDR <0.05) and the effect size (fold-change) for each comparison.

Gene ontology (GO) enrichment analyses were performed using the Cytoscape app ClueGO (version 2.5.3)[51], with the following parameters: only pathways with pV ≤0.01, Minimum GO level =3, Maximum GO level =8, Min GO family >1, minimum number of genes associated to GO term =5, and minimum percentage of genes associated to GO term =8. Enrichment *p*-values were calculated using a hypergeometric test (*p*-value<0.05, Bonferroni corrected).

Gene expression by RT-qPCR

Reverse transcription of mRNA to cDNA was performed using the iScript cDNA Synthesis kit (Bio-Rad), followed by cDNA amplification using the SsoFast EvaGreen Supermix (Bio-Rad). All primers used in this study are listed in **Supplementary Table 5**. Reactions were performed using the CFX96 real-time PCR detection system (Bio-Rad). The relative gene expression levels were assessed according to the $2^{-\Delta\Delta Ct}$ method using *flab2* or *gapdh* as reference gene for *L. interrogans* or human cells, respectively.

Cell culture and infection

HEK-293T and HepG2 cells were cultured in Minimum Essential Medium Eagle (MEME) (Sigma) supplemented with 10% heat-inactivated fetal bovine serum (Sigma) and 2 mM L-glutamine (Gibco). *Leptospira* strains were diluted in this complete cell culture media prior the infection, at a multiplicity of infection (MOI) of 100:1. All chemical compounds used on cells were added 1 hr before the experiment and maintained throughout the duration specified in the figure legend. BAPTA-AM, KN-93, and ML-7 inhibitors were used at 10, 2 and 7 µM, respectively.

Indirect immunofluorescence and live-cell imaging of epithelial cells and hepatocytes.

Epithelial cells and hepatocytes were cultured on glass coverslips (SPL) coated with L-lysine (Sigma) at a concentration of 0.01% in water for a period of 40 min at 37°C. The coverslips were rinsed twice with PBS to remove excess of L-lysine, and the cells were seeded. At the indicated times, the cells were fixed with 4% paraformaldehyde for 15 min at room temperature (RT) and subsequently incubated for 10 min in 0.5% saponin (Sigma) in PBS and for 1 hr in 1% BSA (Sigma) and 0.075% saponin in PBS. The cells were incubated overnight at 4°C with the anti-ZO1 (13663; Cell Signaling), anti-ZO2 (2847; Cell Signaling), anti-JAM1 (82196; Cell Signaling), anti-pan-cadherin (PA5-16766; ThermoFisher) or anti-connexin-43 (3512; Cell Signaling) antibodies at 1:100. Cells were washed and incubated for 1 hr with Alexa Fluor 555 or 488 antibody (ThermoFisher) at 1:500. Filamentous actin was labeled with ActiStain555 phalloidin (PHDH1; Tebu) at 100 nM during 30 min at room temperature. The nuclei were then stained with DAPI (1 µg/mL; ThermoFisher) for 10 min and mounted on a glass side using Fluoromount mounting medium (ThermoFisher). Fluorescence was analyzed using a Leica TCS SP8 Confocal System. The quantification was performed using Icy software in a non-blinded manner.

For live-cell imaging, cells were seeded on an µ-Slide 8 Well (Ibidi). To assess ER activity, cells were labelled with ER-Tracker Red (ThermoFisher) at a concentration of 1 µM for 30 min at 37°C, followed by two washes with FluoroBrite DMEM medium (ThermoFisher) supplemented with 10% heat-inactivated fetal bovine serum (Sigma) and 2 mM L-glutamine (Gibco). For the measurement of intracellular calcium levels, cells were incubated with Fluo-8 AM (Abcam) at a concentration of 4 µM for 1 hr, after which they were washed twice with complete FluoroBrite DMEM medium prior to the analysis time. Brightfield and fluorescence microscopy were conducted using an inverted widefield microscope equipped with an LED colibris and a mercury lamp. Images were acquired using a dual camera sCMOS Hamamatsu ORCA FLASH. Cell dispersion and fluorescence quantification were performed using Icy software (Version 3.0). For each experimental condition, at least 3 random fields and 100 cells were analyzed. Cell boundaries were defined using filamentous actin staining and individual ROIs (region-of-interest) were generated for each cell, where the mean fluorescence intensity of ZO-1, ZO-2, JAM-1, pan-cadherin and connexin-43 was obtained. For pan-cadherin and connexin-43, fluorescence intensity was separately quantified at the plasma membrane and within the ER compartment, defined by FM4-64FX (5 µg/mL; ThermoFisher) and ER-Tracker staining, respectively.

Cell-free area was quantified from confocal images by analyzing 10 randomly selected fields per condition. First, the total cell area within each field was segmented, regions not occupied by cells were identified as cell-free areas and the average distance between medial axis of cell-free area

and the adjacent cell-containing areas was calculated as an index of spacing between cells. To account for differences in cell density, the cell-free area was normalized to the number of cells in each field, providing a relative measure of intercellular spacing per cell.

Cell viability assays

Cell viability was determined using the MTT assay kit (Abcam), according to manufacturer's instructions.

Cell death was evaluated with the Dead Cell Apoptosis Kit with Annexin V Alexa Fluor 488 and Propidium iodide (V13241; ThermoFisher) according to the manufacturer's instructions. Fluorescence was analyzed using a CytoFLEX Flow Cytometer (Beckman Coulter). At least 10,000 events per sample were recorded. A positive control corresponding to cells incubated at 55°C for 20 min prior staining is included for the analysis. The analysis was performed using the Floreada.io website (version SIMD).

Immunoblot

Total extracts of epithelial cells or *Leptospira* strains were obtained by sonication in a lysis buffer containing 25 mM Tris pH 7.5, 100 mM KCl, 2 mM EDTA, 5 mM DTT and a protease inhibitor cocktails (cOmplete Mini EDTA-free, Roche). 10 µg of total proteins were loaded on a 12% SDS-PAGE (Mini-PROTEAN TGX Stain-Free precast gels, Biorad) and transferred onto nitrocellulose membrane. The membranes were blocked with PBS Tween20 0.1% containing 5% BSA for 1 hr at RT and incubated overnight at 4°C with the antibodies anti-ZO1 (13663; Cell Signaling), anti-ZO2 (2847; Cell Signaling), anti-Profilin-1 (3246; Cell Signaling), anti-WAVE-2 (3659; Cell Signaling), anti-pRac1 (2461; Cell Signaling), anti-pCofilin (3313; Cell Signaling), anti-Cofilin (5175; Cell Signaling), anti-GAPDH (5174; Cell Signaling), anti-MLC2 (8505; Cell Signaling), anti-pMLC2 (3671; Cell Signaling), anti-PERK (3192; Cell Signaling), anti-pPERK (PA5-40294; ThermoFisher), anti-IRE1 (3294; Cell Signaling), anti-pIRE1 (PA1-16927; ThermoFisher) and anti-3xFLAG (87537; Cell Signaling) at a 1:1000 dilution. Membranes were washed in PBS-0.1% Tween20 and incubated at RT with secondary HRP-conjugated antibody (7074S; Cell Signaling) at a 1:1000 dilution for 1 hr. Detection was performed with SuperSignal West Femto Maximum Sensitivity Substrate (Thermo Fisher). The molecular mass markers (in kilodaltons) are indicated on the left of each immunoblot panel Quantification of band intensities was performed using ImageJ software.

Translocation through epithelial cells

5.10^4 HEK293T cells in 300 µL of complete MEME were introduced into 12-mm-diameter Transwell filter units with 3 µm pores (COSTAR). The monolayers were incubated at 37°C in 5% CO_2 for a period of three days until the transepithelial resistance reached a range of 200 and 300 Ω/cm2 using an epithelial voltammeter. The monolayers were infected with leptospires at a MOI of 100. At the indicated times, the capacity of *Leptospira* strains to translocate across the epithelial cell barrier was evaluated by extracting the DNA from the bacterial suspension recovered in the lower chamber (300 µL) using the Maxwell RSC Cultured Cells DNA Kit and the Maxwell instrument (Promega). The concentration of leptospires was determined by qPCR with the Sso Fast EvaGreen Supermix assay (Bio-Rad) using *flaB2* (LIMLP_09410) for *L. interrogans* and *flaB4* (LEPBIa1589) for *L. biflexa* (**Supplementary Table 5)**. The capacity of leptospires to translocate HEKT293T polarized monolayers (% of *Leptospira* recovery) was quantified by calculating the proportion of leptospires present in the lower chamber relative to the initial inoculum at each time points.

Complementation of *L. interrogans* mutants

Complementation of the *LIMLP_11660* mutant was performed by expressing LIMLP_11660 using the replicative vector pMaOri[52] (**Supplementary Table 4)** under the control of its native promoter. For this, LIMLP_11660 ORF and the 300 bp upstream region were amplified from genomic DNA of *L. interrogans* (using CompLIMLP_11660 primer set; **Supplementary Table 5)** and cloned between the SacI and NotI restriction sites in the pMaOri vector. The absence of mutations in the resulting plasmid (pMaOri-*LIMLP_11660*, **Supplementary Table 4**) was confirmed by DNA sequencing (Eurofins). Then, the plasmid pMaOri-*LIMLP_11660* was introduced into *LIMLP_11660* mutant strain by conjugation using the *E. coli* β2163 conjugating strain, as previously described[53]. *Leptospira* conjugants were selected on EMJH agar plates containing 50 µg/mL spectinomycin. WT and *LIMLP_11660* mutant strains containing the empty pMaOri vector were used as controls.

Expression of the Flag-tagged LIMLP_11660 variants was performed by introducing a 3xFlag tag in frame at the 3' of the ORF (*LIMLP_11660*$_{comp\text{-}C1}$) or by replacing the peptide signal (*LIMLP_11660*$_{comp\text{-}C2}$) using restriction-free cloning method in the plasmid pMaOri-*LIMLP_11660* with the primers *LIMLP_11660-C1* and *LIMLP_11660-C2* (**Supplementary Table 5**). Conjugation in *L. interrogans* was performed as described above. Gene silencing of *LIMLP_11655* into the *LIMLP_11660* mutant was performed by introducing the leptospiral replicative vector pMaori.dCas9_sg*LIMLP_11655* by conjugation as previously described[11].

Supernatant isolation of *L. interrogans*

Supernatants were obtained from exponentially growing *L. interrogans* cultivated in MEME medium (Sigma) supplemented with 10% heat-inactivated fetal bovine serum (Sigma) and 2 mM L-glutamine (Gibco) overnight at 37°C. Bacteria were centrifuged at 5000 g for 15 min and the supernatants were filtered through a 300 kDa membrane (Sartorius). Unless otherwise indicated in the Figure legends, cells were incubated with supernatants for 24 hrs (in infection experiments or in Transwell assays).

***In silico* analysis of LIMLP_11660 and LIMLP_11655**

The sequence similarity of the LIMLP_11660 protein from *L. interrogans* serovar Manilae was determined using UniProtKB reference proteomes and Swiss-Prot databases. All significant hits, defined as the best match for each species with an e-value <0.00033 and a protein identity >20%, were retained. Sequence alignment of the proteins and percent identity matrix were performed using Clustal-Omega (1.2.4). Tree inference was achieved with IQ-TREE v2.0.6 under the best-fitted model.

The domain models were created using the LIMLP_11660 or LIMLP_11655 protein sequences via the SWISS-MODEL Workspace server (https://swissmodel.expasy.org/, SMTL version 2023-04-05, PDB release 2023-03-31).

Statistics and reproducibility

Statistical analyses were conducted using GraphPad Prism (version 9.5.1). Unless otherwise stated, all experiments were performed in three independent biological replicates. All microscopy images shown are representative of three independent biological replicates. In all graphs, data are presented as mean ± SD. Centre line, median, box limits, the interquartile range ± min and max values were indicated in box and whisker plots. Information about specific statistical tests in each analysis can be found in the figure legends.

DATA AVAILABILITY

The raw fastq files of Dual RNA-sequencing have been deposited in NCBI's Gene Expression Omnibus (GEO, (https://urldefense.com/v3/__https:/www.ncbi.nlm.nih.gov/geo/query/acc.cgi?acc=GSE295802__;!!JFdNOqOXpB6UZW0!sR4HNvjW7T4xwxbEqgJZGtFaMjiKrZTv5ak9KxavvdWnzi4ilMhOFBaWUu0vEL095w7RAiqp-l4Ge0U4ic8$) and are accessible through GEO Series accession number

GSE295802. The data are publicly available without restrictions. Source data are provided with this paper.

REFERENCES

1. Spadoni, I., Fornasa, G. & Rescigno, M. Organ-specific protection mediated by cooperation between vascular and epithelial barriers. *Nat. Rev. Immunol.* **17**, 761–773 (2017).

2. Hartsock, A. & Nelson, W. J. Adherens and Tight Junctions: Structure, Function and Connections to the Actin Cytoskeleton. *Biochim. Biophys. Acta* **1778**, 660–669 (2008).

3. Sousa, S., Lecuit, M. & Cossart, P. Microbial strategies to target, cross or disrupt epithelia. *Curr. Opin. Cell Biol.* **17**, 489–498 (2005).

4. Costa, F. *et al.* Global Morbidity and Mortality of Leptospirosis: A Systematic Review. *PLoS Negl. Trop. Dis.* **9**, e0003898 (2015).

5. Sato, H. & Coburn, J. Leptospira interrogans causes quantitative and morphological disturbances in adherens junctions and other biological groups of proteins in human endothelial cells. *PLoS Negl. Trop. Dis.* **11**, e0005830 (2017).

6. De Brito, T. *et al.* Immunohistochemical and in situ hybridization studies of the liver and kidney in human leptospirosis. *Virchows Arch.* **448**, 576–583 (2006).

7. Wunder, E. A. *et al.* A live attenuated-vaccine model confers cross-protective immunity against different species of the Leptospira genus. *eLife* **10**, e64166 (2021).

8. Tully, C. C. *et al.* Efficacy of minocycline and tigecycline in a hamster model of leptospirosis. *Diagn. Microbiol. Infect. Dis.* **71**, 366–369 (2011).

9. Haake, D. A. Hamster Model of Leptospirosis. *Curr. Protoc. Microbiol.* **CHAPTER**, Unit-12E.2 (2006).

10. Silva, É. F. *et al.* Characterization of virulence of *Leptospira* isolates in a hamster model. *Vaccine* **26**, 3892–3896 (2008).

11. Giraud-Gatineau, A. *et al.* Evolutionary insights into the emergence of virulent Leptospira spirochetes. *PLoS Pathog.* **20**, e1012161 (2024).

12. Li, B. *et al.* Intestinal epithelial tight junctions and permeability can be rescued through the regulation of endoplasmic reticulum stress by amniotic fluid stem cells during necrotizing enterocolitis. *FASEB J.* **35**, e21265 (2021).

13. Huang, Y. *et al.* Role of Endoplasmic Reticulum Stress-Autophagy Axis in Severe Burn-Induced Intestinal Tight Junction Barrier Dysfunction in Mice. *Front. Physiol.* **10**, 606 (2019).

14. Seo, S. H., Kim, S.-E. & Lee, S. E. ER stress induced by ER calcium depletion and UVB irradiation regulates tight junction barrier integrity in human keratinocytes. *J. Dermatol. Sci.* **98**, 41–49 (2020).

15. Vasioukhin, V., Bauer, C., Yin, M. & Fuchs, E. Directed Actin Polymerization Is the Driving Force for Epithelial Cell–Cell Adhesion. *Cell* **100**, 209–219 (2000).

16. Van Itallie, C. M., Fanning, A. S., Bridges, A. & Anderson, J. M. ZO-1 Stabilizes the Tight Junction Solute Barrier through Coupling to the Perijunctional Cytoskeleton. *Mol. Biol. Cell* **20**,

3930–3940 (2009).

17. Shen, L. *et al.* Myosin light chain phosphorylation regulates barrier function by remodeling tight junction structure. *J. Cell Sci.* **119**, 2095–2106 (2006).

18. Cunningham, K. E. & Turner, J. R. Myosin light chain kinase: pulling the strings of epithelial tight junction function. *Ann. N. Y. Acad. Sci.* **1258**, 34–42 (2012).

19. Chaurasia, R. & Vinetz, J. M. In silico prediction of molecular mechanisms of toxicity mediated by the leptospiral PF07598 gene family-encoded virulence-modifying proteins. *Front. Mol. Biosci.* **9**, 1092197 (2023).

20. Wunder, E. A. *et al.* Real-Time PCR Reveals Rapid Dissemination of Leptospira interrogans after Intraperitoneal and Conjunctival Inoculation of Hamsters. *Infect. Immun.* **84**, 2105–2115 (2016).

21. Damron, F. H., Oglesby-Sherrouse, A. G., Wilks, A. & Barbier, M. Dual-seq transcriptomics reveals the battle for iron during Pseudomonas aeruginosa acute murine pneumonia. *Sci. Rep.* **6**, 39172 (2016).

22. Demiroz, D. *et al.* Listeria monocytogenes infection rewires host metabolism with regulatory input from type I interferons. *PLOS Pathog.* **17**, e1009697 (2021).

23. Mai, D. *et al.* Exposure to Mycobacterium remodels alveolar macrophages and the early innate response to Mycobacterium tuberculosis infection. *PLOS Pathog.* **20**, e1011871 (2024).

24. Wuerth, K., Lee, A. H. Y., Falsafi, R., Gill, E. E. & Hancock, R. E. W. Characterization of Host Responses during Pseudomonas aeruginosa Acute Infection in the Lungs and Blood and after Treatment with the Synthetic Immunomodulatory Peptide IDR-1002. *Infect. Immun.* **87**, e00661-18 (2018).

25. Brady, R. A., Bruno, V. M. & Burns, D. L. RNA-Seq Analysis of the Host Response to Staphylococcus aureus Skin and Soft Tissue Infection in a Mouse Model. *PLoS ONE* **10**, e0124877 (2015).

26. Minhas, V. *et al.* In vivo dual RNA-seq reveals that neutrophil recruitment underlies differential tissue tropism of Streptococcus pneumoniae. *Commun. Biol.* **3**, 293 (2020).

27. Fraga, T. R., Isaac, L. & Barbosa, A. S. Complement Evasion by Pathogenic Leptospira. *Front. Immunol.* **7**, 623 (2016).

28. Werts, C. *et al.* Leptospiral lipopolysaccharide activates cells through a TLR2-dependent mechanism. *Nat. Immunol.* **2**, 346–352 (2001).

29. Santecchia, I. *et al.* Alive Pathogenic and Saprophytic Leptospires Enter and Exit Human and Mouse Macrophages With No Intracellular Replication. *Front. Cell. Infect. Microbiol.* **12**, 936931 (2022).

30. Reis, E. A. G. *et al.* Cytokine Response Signatures in Disease Progression and Development of Severe Clinical Outcomes for Leptospirosis. *PLoS Negl. Trop. Dis.* **7**, e2457 (2013).

31. Conroy, A. L. *et al.* Host biomarkers distinguish dengue from leptospirosis in Colombia: a case–control study. *BMC Infect. Dis.* **14**, 35 (2014).

32. Chirathaworn, C., Supputtamongkol, Y., Lertmaharit, S. & Poovorawan, Y. Cytokine levels as biomarkers for leptospirosis patients. *Cytokine* **85**, 80–82 (2016).

33. O'Grady, N. P. *et al.* Detection of Macrophage Inflammatory Protein (MIP)-1α and MIP-β during Experimental Endotoxemia and Human Sepsis. *J. Infect. Dis.* **179**, 136–141 (1999).

34. Kleinertz, H. *et al.* Circulating growth/differentiation factor 15 is associated with human CD56bright natural killer cell dysfunction and nosocomial infection in severe systemic inflammation. *eBioMedicine* **43**, 380–391 (2019).

35. Chandra, P., Grigsby, S. J. & Philips, J. A. Immune evasion and provocation by Mycobacterium tuberculosis. *Nat. Rev. Microbiol.* **20**, 750–766 (2022).

36. Figueiredo, P. de, Ficht, T. A., Rice-Ficht, A., Rossetti, C. A. & Adams, L. G. Pathogenesis and Immunobiology of Brucellosis: Review of Brucella–Host Interactions. *Am. J. Pathol.* **185**, 1505–1517 (2015).

37. Huber, P. Targeting of the apical junctional complex by bacterial pathogens. *Biochim. Biophys. Acta BBA - Biomembr.* **1862**, 183237 (2020).

38. Sebastián, I. *et al.* Disassembly of the apical junctional complex during the transmigration of Leptospira interrogans across polarized renal proximal tubule epithelial cells. *Cell. Microbiol.* **23**, e13343 (2021).

39. Nuss, A. M. *et al.* Tissue dual RNA-seq allows fast discovery of infection-specific functions and riboregulators shaping host–pathogen transcriptomes. *Proc. Natl. Acad. Sci.* **114**, E791–E800 (2017).

40. Steed, E., Balda, M. S. & Matter, K. Dynamics and functions of tight junctions. *Trends Cell Biol.* **20**, 142–149 (2010).

41. Lehmann, J. S. *et al.* Pathogenomic Inference of Virulence-Associated Genes in Leptospira interrogans. *PLoS Negl. Trop. Dis.* **7**, e2468 (2013).

42. Costa, T. R. D. *et al.* Secretion systems in Gram-negative bacteria: structural and mechanistic insights. *Nat. Rev. Microbiol.* **13**, 343–359 (2015).

43. Cokelaer, T., Desvillechabrol, D., Legendre, R. & Cardon, M. 'Sequana': a Set of Snakemake NGS pipelines. *J. Open Source Softw.* **2**, 352 (2017).

44. Köster, J. & Rahmann, S. Snakemake—a scalable bioinformatics workflow engine. *Bioinformatics* **28**, 2520–2522 (2012).

45. Chen, S., Zhou, Y., Chen, Y. & Gu, J. fastp: an ultra-fast all-in-one FASTQ preprocessor. *Bioinformatics* **34**, i884–i890 (2018).

46. Langmead, B. & Salzberg, S. L. Fast gapped-read alignment with Bowtie 2. *Nat. Methods* **9**, 357–359 (2012).

47. Dobin, A. *et al.* STAR: ultrafast universal RNA-seq aligner. *Bioinforma. Oxf. Engl.* **29**, 15–21 (2013).

48. Liao, Y., Smyth, G. K. & Shi, W. featureCounts: an efficient general purpose program for assigning sequence reads to genomic features. *Bioinformatics* **30**, 923–930 (2014).

49. Ewels, P., Magnusson, M., Lundin, S. & Käller, M. MultiQC: summarize analysis results for multiple tools and samples in a single report. *Bioinformatics* **32**, 3047–3048 (2016).

50. Love, M. I., Huber, W. & Anders, S. Moderated estimation of fold change and dispersion for RNA-seq data with DESeq2. *Genome Biol.* **15**, 550 (2014).

51. Bindea, G. *et al.* ClueGO: a Cytoscape plug-in to decipher functionally grouped gene ontology and pathway annotation networks. *Bioinformatics* **25**, 1091–1093 (2009).

52. Pappas, C. J., Benaroudj, N. & Picardeau, M. A Replicative Plasmid Vector Allows Efficient Complementation of Pathogenic Leptospira Strains. *Appl. Environ. Microbiol.* **81**, 3176

(2015).

53. Picardeau, M. Conjugative Transfer between Escherichia coli and Leptospira spp. as a New Genetic Tool. *Appl. Environ. Microbiol.* **74**, 319–322 (2008).

ACKNOWLEDGEMENTS

This work has received financial support by the PTR (Programmes Transversaux de Recherche) grant (PTR2019-310) from Institut Pasteur Paris (to NB), by a Groot-23 from the department of Microbiology of Institut Pasteur Paris (to AGG), and by the National Institutes of Health grant P01 AI 168148 (to MP & NB). We thank the Ultrastructural BioImaging Platform (UTechS UBI, Institut Pasteur Paris) for technical support. We also acknowledge L. Lemée and R. Ouazahrou from Biomics Platform, C2RT, Institut Pasteur, Paris, France, supported by France Génomique (ANR-10-INBS-09) and IBISA for their technical help for RNASeq experiments. We are grateful to N. Sauvonnet, E. Lemichez, L. Tailleux, and M. Lago for critically reading the manuscript and helpful discussions. The funders had no role in study design, data collection and analysis, decision to publish, or preparation of the manuscript.

AUTHOR CONTRIBUTIONS

N.B. and A.G-G. conceptualized the study and designed the experiments. N.B. supervised the study. A.G-G. conducted most of the experiments. G.H. prepared the samples for and performed the RNA sequencing. M.M. performed the analyses of the RNASeq data. M.P. performed gene inactivation and silencing. A.G-G, G.H., M.M., M.P. and N.B. validated the data and analyses. N.B., M.P., A.G-G., and M.M. participated in funding acquisition. A.G-G and N.B. wrote the original draft. All authors reviewed, edited and approved the final manuscript.

COMPETING INTERESTS

The authors declare no competing interests.

FIGURE LEGENDS

Figure 1. Design and evaluation of the *in vivo* Dual RNA-seq for *L. interrogans*-infected hamsters

(**A**) Survival of hamsters infected with *L. interrogans*. The virulence *of L. interrogans* was evaluated in hamsters (n=4) via an intraperitoneal infection with 10^8 leptospires.

(**B**) Leptospiral burden in kidneys and liver was quantified by qPCR and expressed as genomic equivalents (GEq) per μg of hamster DNA. Data are the mean ± SD of four biological replicates and statistical significance was determined by one-way ANOVA test compared to 1 dpi. *, p=0.0308; ***, p<0.0001.

(**C**) Schematic description of the dual RNA-seq workflow. Hamsters were infected with *L. interrogans* by intraperitoneal route. At 1 and 3 dpi, RNAs were extracted from liver and kidney tissues, and sequenced. In parallel, RNA extraction and sequencing were performed on exponentially growing *L. interrogans* cultivated in EMJH medium. Host responses were analyzed by comparing transcriptomes of infected versus uninfected tissues. A deep RNA-sequencing was performed on samples isolated from liver at 3 dpi (n= 3) to enrich bacterial reads and enable comparison of *L. interrogans* transcriptional profiles *in vivo* and *in vitro*. Hamster and leptospiral RNAs were represented in blue and red, respectively. This illustration was created using BioRender (GIRAUD GATINEAU, A. (2026) https://BioRender.com/s6zt1w8).

(**D**) Principal component analysis (PCA) of the global gene expression in liver and kidney upon *L. interrogans* infection at 1 and 3 dpi. Uninfected conditions are presented by light green (1 dpi) and light red (3 dpi) symbols. The numbers of differentially expressed genes (DEGs) (FDR ≤0.05; $|Log_2FC| \geq 1$) in liver and kidneys at 1- and 3-dpi are indicated.

(**E**) Proportion of *L. interrogans* genes detected in each dataset (at 3 dpi; only genes with at least one read mapped in each biological replicate are considered), highlighting the enrichment achieved through deep sequencing, and PCA of the global gene expression of *L. interrogans* in liver at 3 dpi compared to EMJH condition. The numbers of leptospiral DEGs (FDR ≤0.05; $|Log_2FC| \geq 1$) in hamster liver compared to EMJH condition are indicated.

Source data are provided as a Source Data file.

Figure 2. Host transcriptional response to *L. interrogans* infection *in vivo*.

(**A**) KEGG analysis of major upregulated and downregulated pathways in liver and kidneys at 3 dpi. The y-axis shows the enriched pathways and the x-axis values are the mean Log_2FC ± SD of the DEGs in each enriched pathway from three biological replicates. Up- and downregulated ORFs are represented by red and blue symbols, respectively.

(**B**) Heatmap showing DEGs related to Cytokine-cytokine receptor interaction (upper panel) and Chemokine signaling pathway (lower panel) in liver and kidneys upon *L. interrogans* infection. Gene names are indicated at the bottom of the panels. Differential expressions are expressed as Log_2FC (infected versus uninfected) with a heat map color from blue to red indicating low to high Log_2FC.

(**C**) KEGG pathways analysis of DEGs in *L. interrogans*-infected hamsters involved in cytoskeleton organization Gene Ontology group. Only the ten most significative pathways are represented (with a *p*-value corrected with Bonferroni step down <0.005). The percentage of DEGs associated with each pathway is indicated for the liver (in green) and kidneys (in brown).

Source data are provided as a Source Data file.

Figure 3. Transcriptional landscape of *L. interrogans in vivo*

(**A**) Volcano representation of *L. interrogans* DEGs in liver of infected hamsters (n=3) at 3 dpi compared to *L. interrogans* cultivated in EMJH medium (n=3). Up- and downregulated ORFs are represented in red and blue, respectively, and genes that are not significantly differentially expressed are shown in grey (FDR ≤0.05; $|Log_2FC| \geq 1$). Reported *p*-values are two-sided and adjusted for multiple comparisons using the Benjamini-Hochberg false discovery rate (*p*-values adjusted). The locus name of the two most upregulated genes under *in vivo* condition is indicated.

(**B**) KEGG analysis of the most deregulated pathways in *L. interrogans* in liver of infected hamsters at 3 dpi. The y-axis shows enriched pathways and values of the x-axis are the mean $Log_2FC \pm SD$ of DEGs for each enriched pathway from three biological replicates. The number of DEGs for each pathway is represented in the right panel. Up- and downregulated ORFs are represented in red and blue, respectively.

(**C**) Heatmaps of selected up- and downregulated genes under *in vivo* condition (*L. interrogans* DEGs in liver of infected hamsters at 3 dpi versus *L. interrogans* cultivated in EMJH medium). Genes were classified using COG annotation. Gene names and nomenclatures are indicated on the left of each panel. Differential expressions are expressed as Log_2FC (*L. interrogans* in liver of infected hamsters at 3 dpi versus *L. interrogans* cultivated in EMJH medium) with a heat map color from blue to red indicating low to high Log_2FC.

Source data are provided as a Source Data file.

Figure 4. *L. interrogans* infection induces actin cytoskeletal remodeling in human epithelial cells without causing cell death.

(**A-B**) Phase contrast (A) and confocal (B) images of epithelial cells uninfected or infected with *L. interrogans* for 24 hr. Scale bars: 20 µm (phase contrast) and 10 µm (confocal). Cells were stained for F-actin (in green) and DNA (in blue) for confocal images. These images are representative of 3 biological replicates.

(**C**) Quantification of cell-free area for uninfected (empty symbols) or infected condition (blue symbols) (n=10 fields). Box and whisker plots represent median and interquartile range ± min and max values, respectively, from 3 biological experiments. ****, $p<0.0001$ (unpaired, two-tailed *t* test).

(**D**) Percentages of apoptotic and necrotic epithelial cells after *L. interrogans* infection. Fluorescence intensity was quantified by flow cytometry (n=10,000 cells). Data represent mean ± SD from 3 biological replicates. ***, $p=0.0001$; ****, $p\leq0.0001$ (unpaired, two-tailed *t* test).

Source data are provided as a Source Data file.

Figure 5. *L. interrogans* infection disrupts cell-cell junctions in human epithelial cells. (**A**) Confocal images of uninfected or *L. interrogans*-infected cells (24 hr), stained for pan-cadherin (in red) and DNA (in blue), with corresponding fluorescence quantification of plasma membrane-associated cadherin. Scale bars, 20 µm. Data represent the mean ± SD from 3 biological replicates. ****, $p<0.0001$ (unpaired, two-tailed *t* test).

(**B-C**) Confocal images of uninfected and *L. interrogans*-infected cells (B) (24 hr), stained for ZO-1, ZO-2 or JAM-1 (in red) and DNA (in blue) with corresponding quantification of fluorescence intensity per cell (C) (n=100 cells). Scale bars, 20 µm. Data represent the mean ± SD and are representative of 3 biological replicates. ****, $p<0.0001$ (unpaired, two-tailed *t* test).

(**D**) Immunoblot analysis of ZO-1 and ZO-2 in uninfected (UNI) and infected (INF) cells. GAPDH cellular content was used as an equal loading control. Relative protein levels in infected cells (normalized to uninfected controls) are shown. Data are from 2 independent experiments.

(**E-G**) Confocal images of uninfected and *L. interrogans*-infected cells (24 hr) stained for Connexin-43 (in red), plasma membrane (in green), ER (in grey) and DNA (in blue) (E), with quantification of Connexin-43 intensity per cell (F) (n=100 cells) and the colocalization of Connexin-43 in the plasma membrane and ER (G) (n=100 cells). Scale bars, 20 µm. Data represent the mean ± SD and are representative of 3 biological replicates. ns, not significant with $p=0.8196$; ****, $p<0.0001$ (unpaired, two-tailed *t* test).

(**H**) Ability of *L. interrogans* and *L. biflexa* to translocate through human epithelial cell monolayers measured by a transwell assay. % of *Leptospira* recovered in the lower chamber obtained by qPCR at the indicated times were normalized by those of the inoculum. *L. biflexa* were used as

negative controls. Data are mean ± SD from 3 independent experiments. ***, p=0.0001; ****, p<0.0001 (unpaired, two-tailed t test).
Images in (A), (B) and (E) are representative of 3 biological replicates.
Source data are provided as a Source Data file.

Figure 6. Regulation of intracellular Ca^{2+} concentration in human epithelial cells during infection by *L. interrogans*.

(**A**) Live images of HEK293T cells infected (lower panels) or not (upper panels) with *L. interrogans* for 0, 24 or 48 hr and stained with Fluo-8 AM (in green) to visualize free Ca^{2+}. Scale bars, 10 µm. The images are representative of 3 biological replicates.

(**B**) Quantification of the Fluo-8 AM intensity per cell at 0, 24 and 48 hr pi (n=100 cells per condition). Values obtained for infected cells (blue symbols) were normalized to that of uninfected cells (empty symbols) at 0 hr. Data represent the mean ± SD, representative of 3 biological replicates. ns, not significant with p=0.7921; ****, p<0.0001 (one-way ANOVA test).

(**C**) Quantification of the Fluo-8 AM intensity per cell in human epithelial cells infected or not with *L. interrogans* at 24 hr pi using flow cytometry (n=10,000 cells per condition). Data of the right panel represent the mean ± SD of 3 biological replicates. *, p=0.0185 (unpaired, two-tailed t test).
Source data are provided as a Source Data file.

Figure 7. Disruption of cell-cell junctions is partially induced by the calcium signaling pathway through calmodulin and MLCK activities during *L. interrogans* infection.

(**A-C**) Confocal images of epithelial cells infected or not with *L. interrogans* for 24 hr (A), treated with the intracellular calcium chelator BAPTA-AM and stained for F-actin (in green), ZO-1 (in red) and DNA (in blue). Scale bars, 10 µm. The quantification of free cell area (n=10 fields) and ZO-1 intensity per cell (n=100 cells per condition) are shown in (B) and (C), respectively. Data in (B) are the median with interquartile range (box and whisker plots) ± min and max values and data in (C) are the mean ± SD. Data are representative of 3 biological replicates. ns, not significant with p=0.8300 and p=0.8844 in (B) and (C), respectively; ****, p<0.0001 (one-way ANOVA test).

(**D**) Immunoblot detection of phosphorylated Myosin (pMLC2), Myosin (MLC2) and GAPDH in infected cells (INF) or not (UNI) after 24 hr. The data are representative of 3 biological replicates. Relative pMLC2/MLC2 levels normalized to uninfected controls are shown. Data are mean ± SD from 3 independent experiments. **, p=0.0100 (unpaired, two-tailed t test).

(**E-G**) Confocal images of uninfected or *L. interrogans*-infected cells (E), treated or not with the calmodulin (KN-93) or MLCK (ML-7) inhibitors for 24 hr, and stained for ZO-1 and DNA. Scale

bars, 20 µm. ZO-1 intensity per cell normalized to the uninfected untreated condition (n=100 cells per condition) and percentage of cell-free area (n=10 fields) were quantified in (F) and (G), respectively. Data are mean ± SD (F) or median with interquartile range (box and whisker plots) ± min and max values (G), representative of 3 biological replicates. ****; p<0.0001 (one-way ANOVA test).

(**H**) Translocation of *L. interrogans* across epithelial cells untreated or treated with BAPTA-AM, KN-93 or ML-7 inhibitors. Data are mean ± SD from 3 independent experiments. **, p=0.0050 (one-way ANOVA test).

The images in (A), (D), and (E) are representative of 3 biological replicates.

Source data are provided as a Source Data file.

Figure 8. VM proteins are required for virulence of *L. interrogans*.

Survival of hamsters (n =4) infected intraperitoneally with 10^8 *L. interrogans* WT, LIMLP_11660 knockout (*LIMLP_11660*) and the corresponding complemented strain ($LIMLP\_11660_{comp}$), or a double LIMLP_11660 and LIMLP_11655 mutant (*LIMLP_11660*+dcas9-*LIMLP_11655*) (see Supplementary Table 3 for a complete description of the bacterial strains). Statistical significance in comparison with the WT strain was determined by a Log rank Mantel Cox test (***, p=0.00815). Source data are provided as a Source Data file.

Figure 9. Secreted leptospiral VM proteins mediate cell-cell junction disruption via calcium regulation.

(**A**) Transwell assay of *L. interrogans* WT and mutant strains (see Supplementary Table 3 for a complete description) through human epithelial cell. Percentage of *Leptospira* recovered in the lower chamber obtained by qPCR were normalized by those of the WT strain. Data are mean ± SD from 3 independent experiments. ***, p=0.0110; ****, p<0.0001 (one-way ANOVA test).

(**B**) Transwell assay of *L. biflexa* through human epithelial cells pre-incubated or not with the supernatants from *L. interrogans* cultures (as in A). Percentage of *Leptospira* recovered in the lower chamber obtained by qPCR were normalized by that of the untreated condition. Data are mean ± SD from 3 independent experiments. ns, not significant with p>0.9999; *, p<0.0318; ***, p=0.0004; ****, p<0.0001 (one-way ANOVA test).

(**C**) Confocal images of epithelial cells incubated with the supernatant from *L. interrogans* cultures (strains as in A-B) for 24 hr and stained for ZO-1 and DNA with corresponding quantified ZO-1 intensity per cell (n=100 cells) normalized by the untreated condition. Scale bars, 20 µm. ns, not significant with p>0.9791; ****, p<0.0001 (one-way ANOVA test).

(**D**) Immunoblot detection of FLAG-tagged LIMLP_11660 in whole bacterial pellets or culture supernatants of the different complemented *LIMLP_11660* mutant strains (constructs are depicted on the left, see Supplementary Table 4 for a complete description).
(**E**) Immunoblot detection of FLAG-tagged LIMLP_11660 (red arrow) in host cells incubated with the supernatants of *L. interrogans* cultures (as in D) for 1- and 6 hr. LIMLP_11660$_{comp\text{-}C1}$ in the *L. interrogans* pellet is used as a positive control. The lower band corresponds to a non-specific recognition.
(**F**) Live images of epithelial cells incubated for 24 hr with the supernatants from *L. interrogans* cultures (strains as described in C) and stained with Fluo-8 AM to visualize free Ca^{2+} with corresponding quantified Fluo-8 AM intensity per cell (n=100 cells per condition) normalized to values in untreated cells. Scale bars, 10 µm. ****, p<0.0001 (one-way ANOVA test).
The data in (C-F) are representative of 3 biological replicates.
Source data are provided as a Source Data file.

Figure 10. Proposed model of VM protein-mediated disruption of cell-cell junctions.
In non-infected cells (on the left), tight junctions (JAM, Occludin and Claudin) and adherens junctions (Cadherin) stabilize cell-cell junctions while ZO/Cadherin proteins connect junctions and actin cytoskeleton. During leptospiral infection (on the right), *L. interrogans* induces the expression and secretion of two virulence-modifying (VM) proteins, LIMLP_11655 and LIMLP_11660. These proteins would interact directly with host epithelial cells, very likely by binding of their Ricin B domain to lectin receptors present at the host cell surface. The VMs could be then internalized within the host cell, where they trigger an increase in intracellular calcium levels. This calcium deregulation would activate the calmodulin-MLCK pathway, leading to actin cytoskeleton remodeling and ultimately disassembly of tight and adherens junctions. The resulting loss of barrier integrity facilitates *L. interrogans* transmigration across epithelial and endothelial cell layers, promoting systemic dissemination to target organs, such as liver and kidneys. This illustration was created using BioRender (GIRAUD GATINEAU, A. (2026) https://BioRender.com/r8e6v70).

Editorial Summary –

Here, the authors use *in vivo* dual RNA sequencing to determine the host-pathogen transcriptomic landscape upon infection by *Leptospira interrogans*, revealing alterations in pathways associated with paracellular permeability, like cell-cell junctions.

Peer review information: *Nature Communications* thanks Maria Gomes-Solecki, Fernando Navarro-Garciaand, Meera Unnikrishnan and the other, anonymous, reviewer(s) for their contribution to the peer review of this work. A peer review file is available.

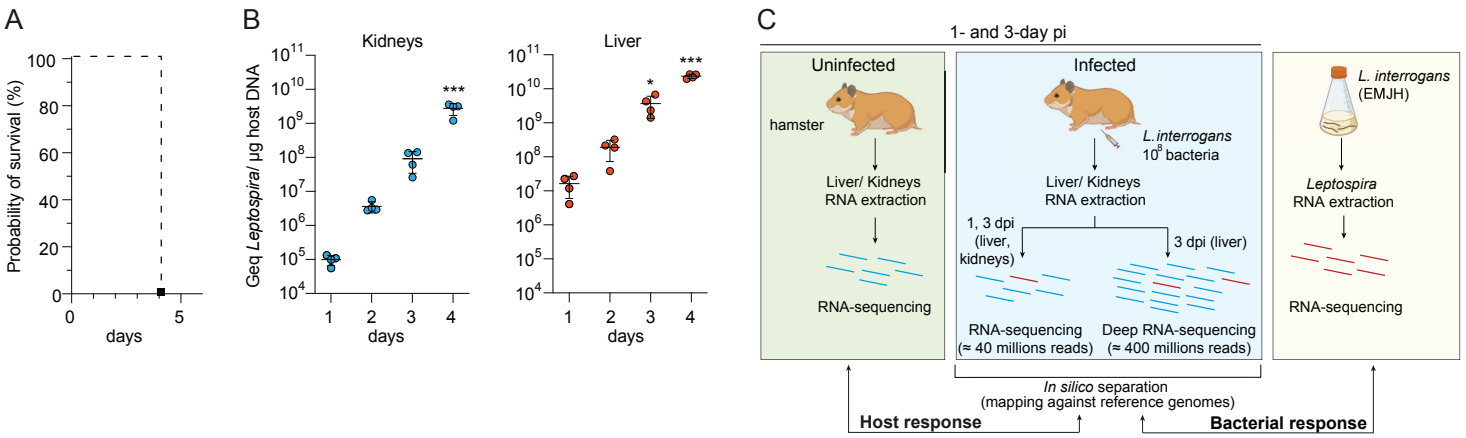

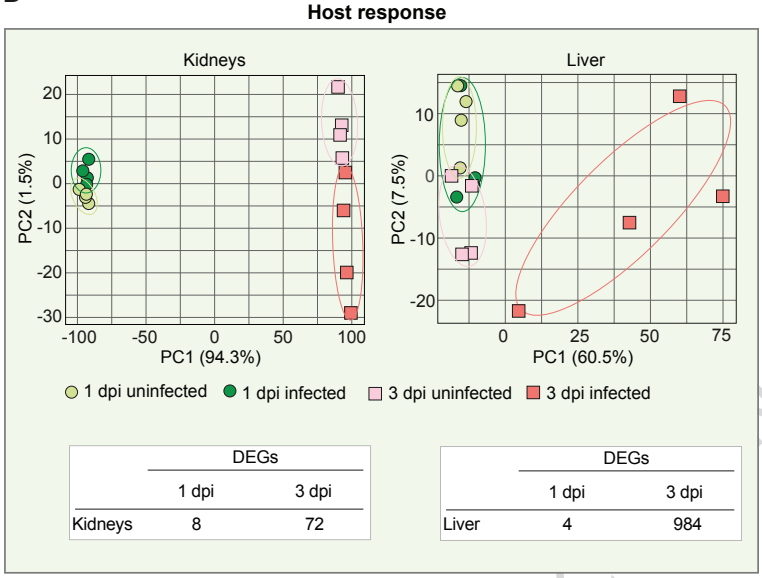

DEGs	1 dpi	3 dpi
Kidneys	8	72

DEGs	1 dpi	3 dpi
Liver	4	984

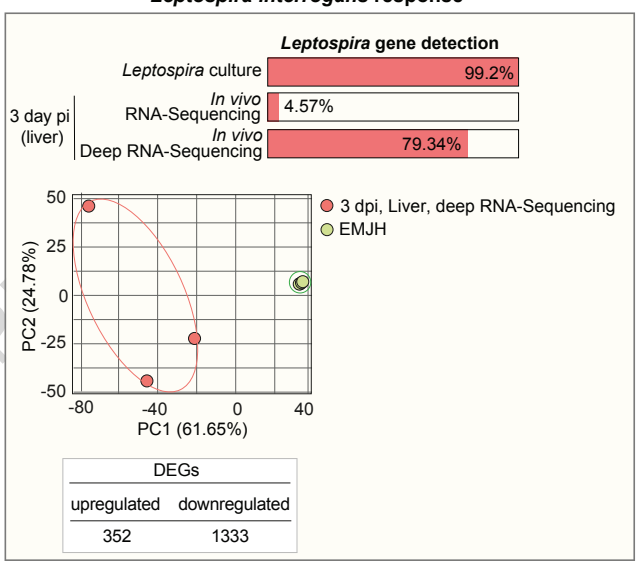

DEGs	upregulated	downregulated
	352	1333

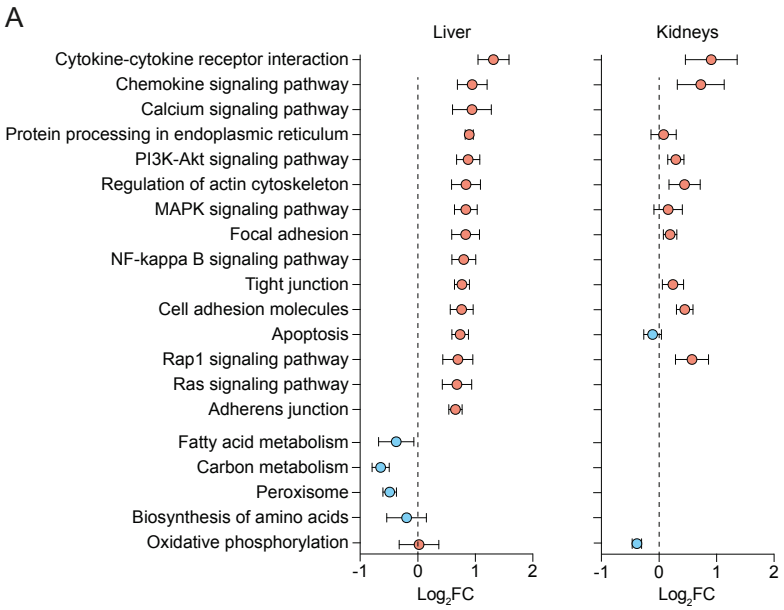

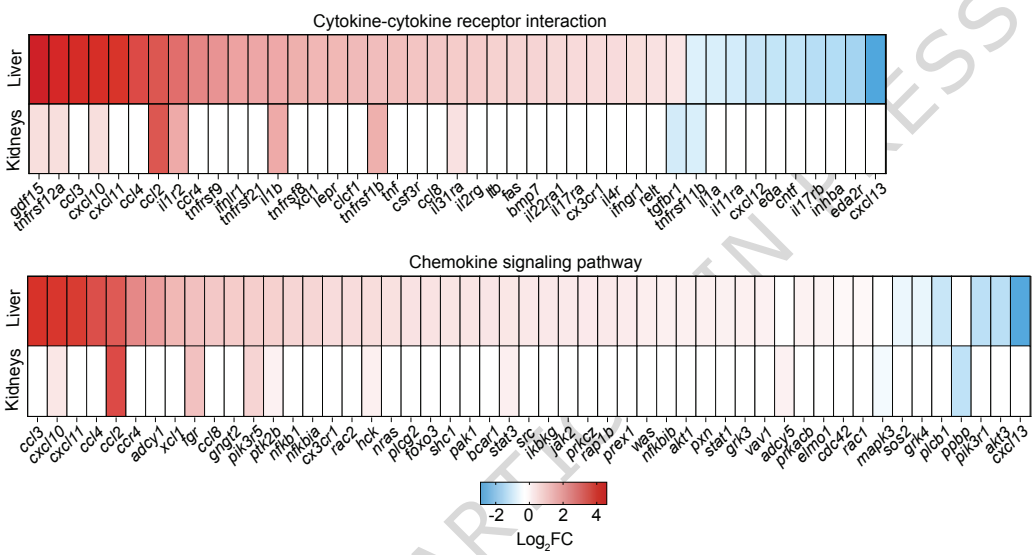

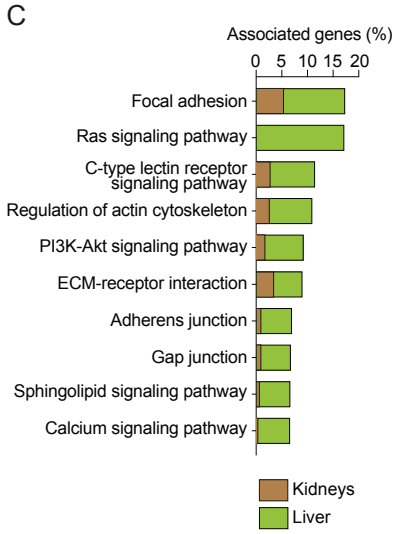

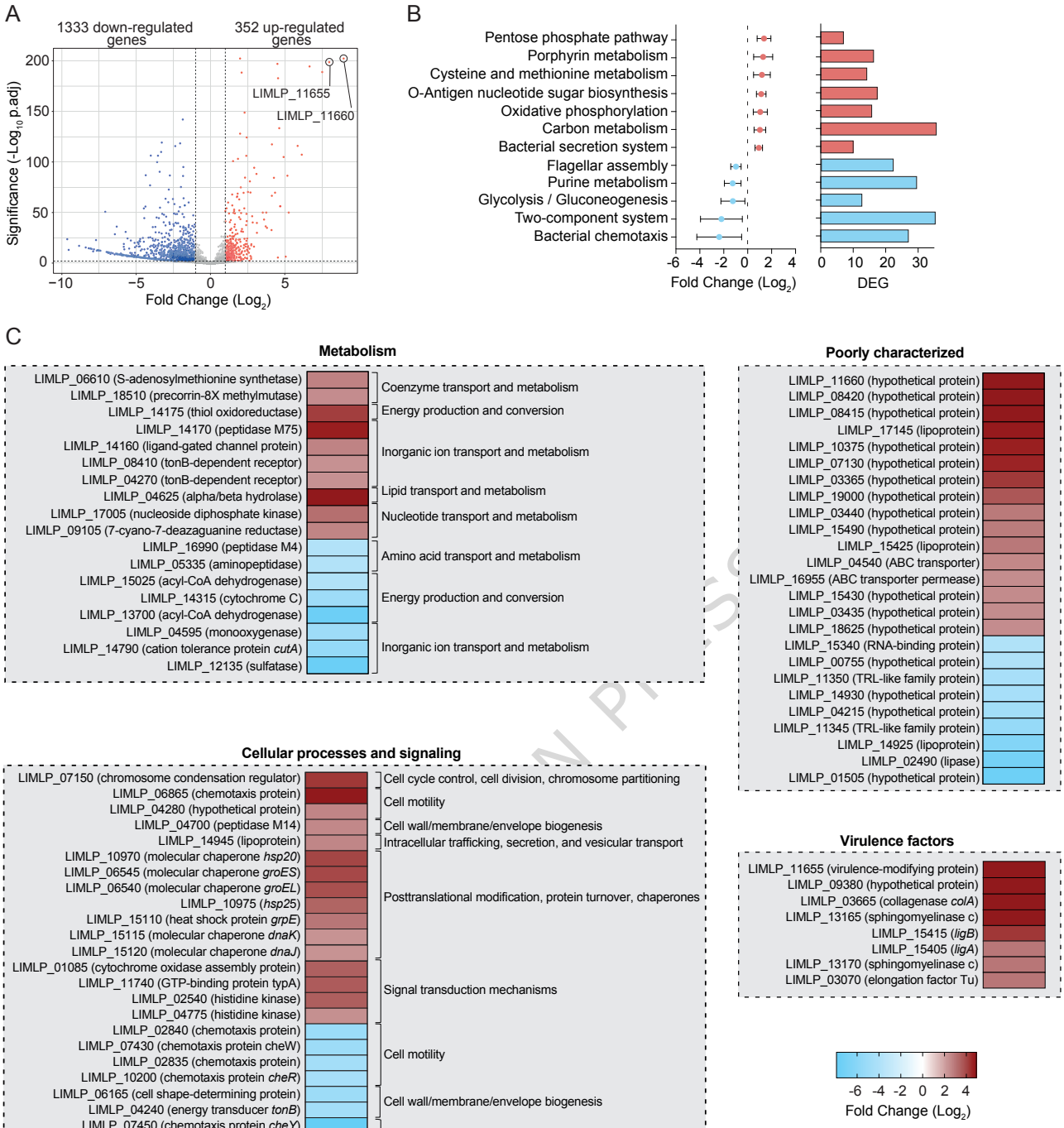
A
1333 down-regulated genes
352 up-regulated genes
LIMLP_11655
LIMLP_11660
Significance (-Log10 p.adj)
Fold Change (Log2)
B
Pentose phosphate pathway
Porphyrin metabolism
Cysteine and methionine metabolism
O-Antigen nucleotide sugar biosynthesis
Oxidative phosphorylation
Carbon metabolism
Bacterial secretion system
Flagellar assembly
Purine metabolism
Glycolysis / Gluconeogenesis
Two-component system
Bacterial chemotaxis
Fold Change (Log2)
DEG
C
Metabolism
LIMLP_06610 (S-adenosylmethionine synthetase)
LIMLP_18510 (precorrin-8X methylmutase)
LIMLP_14175 (thiol oxidoreductase)
LIMLP_14170 (peptidase M75)
LIMLP_14160 (ligand-gated channel protein)
LIMLP_08410 (tonB-dependent receptor)
LIMLP_04270 (tonB-dependent receptor)
LIMLP_04625 (alpha/beta hydrolase)
LIMLP_17005 (nucleoside diphosphate kinase)
LIMLP_09105 (7-cyano-7-deazaguanine reductase)
LIMLP_16990 (peptidase M4)
LIMLP_05335 (aminopeptidase)
LIMLP_15025 (acyl-CoA dehydrogenase)
LIMLP_14315 (cytochrome C)
LIMLP_13700 (acyl-CoA dehydrogenase)
LIMLP_04595 (monooxygenase)
LIMLP_14790 (cation tolerance protein cutA)
LIMLP_12135 (sulfatase)
Coenzyme transport and metabolism
Energy production and conversion
Inorganic ion transport and metabolism
Lipid transport and metabolism
Nucleotide transport and metabolism
Amino acid transport and metabolism
Energy production and conversion
Inorganic ion transport and metabolism
Poorly characterized
LIMLP_11660 (hypothetical protein)
LIMLP_08420 (hypothetical protein)
LIMLP_08415 (hypothetical protein)
LIMLP_17145 (lipoprotein)
LIMLP_10375 (hypothetical protein)
LIMLP_07130 (hypothetical protein)
LIMLP_03365 (hypothetical protein)
LIMLP_19000 (hypothetical protein)
LIMLP_03440 (hypothetical protein)
LIMLP_15490 (hypothetical protein)
LIMLP_15425 (lipoprotein)
LIMLP_04540 (ABC transporter)
LIMLP_16955 (ABC transporter permease)
LIMLP_15430 (hypothetical protein)
LIMLP_03435 (hypothetical protein)
LIMLP_18625 (hypothetical protein)
LIMLP_15340 (RNA-binding protein)
LIMLP_00755 (hypothetical protein)
LIMLP_11350 (TRL-like family protein)
LIMLP_14930 (hypothetical protein)
LIMLP_04215 (hypothetical protein)
LIMLP_11345 (TRL-like family protein)
LIMLP_14925 (lipoprotein)
LIMLP_02490 (lipase)
LIMLP_01505 (hypothetical protein)
Cellular processes and signaling
LIMLP_07150 (chromosome condensation regulator)
LIMLP_06865 (chemotaxis protein)
LIMLP_04280 (hypothetical protein)
LIMLP_04700 (peptidase M14)
LIMLP_14945 (lipoprotein)
LIMLP_10970 (molecular chaperone hsp20)
LIMLP_06545 (molecular chaperone groES)
LIMLP_06540 (molecular chaperone groEL)
LIMLP_10975 (hsp25)
LIMLP_15110 (heat shock protein grpE)
LIMLP_15115 (molecular chaperone dnaK)
LIMLP_15120 (molecular chaperone dnaJ)
LIMLP_01085 (cytochrome oxidase assembly protein)
LIMLP_11740 (GTP-binding protein typA)
LIMLP_02540 (histidine kinase)
LIMLP_04775 (histidine kinase)
LIMLP_02840 (chemotaxis protein)
LIMLP_07430 (chemotaxis protein cheW)
LIMLP_02835 (chemotaxis protein)
LIMLP_10200 (chemotaxis protein cheR)
LIMLP_06165 (cell shape-determining protein)
LIMLP_04240 (energy transducer tonB)
LIMLP_07450 (chemotaxis protein cheY)
LIMLP_16820 (histidine kinase)
LIMLP_07445 (anti-sigma factor antagonist)
LIMLP_11010 (histidine kinase)
LIMLP_16820 (histidine kinase)
LIMLP_07030 (histidine kinase)
LIMLP_07025 (histidine kinase)
LIMLP_01925 (anti-sigma factor antagonist)
LIMLP_10185 (histidine kinase)
LIMLP_10190 (histidine kinase)
LIMLP_05845 (diguanylate phosphodiesterase)
Cell cycle control, cell division, chromosome partitioning
Cell motility
Cell wall/membrane/envelope biogenesis
Intracellular trafficking, secretion, and vesicular transport
Posttranslational modification, protein turnover, chaperones
Signal transduction mechanisms
Cell motility
Cell wall/membrane/envelope biogenesis
Signal transduction mechanisms
Virulence factors
LIMLP_11655 (virulence-modifying protein)
LIMLP_09380 (hypothetical protein)
LIMLP_03665 (collagenase colA)
LIMLP_13165 (sphingomyelinase c)
LIMLP_15415 (ligB)
LIMLP_15405 (ligA)
LIMLP_13170 (sphingomyelinase c)
LIMLP_03070 (elongation factor Tu)
Fold Change (Log2)